

Fractal Analysis of Permeabilities for Porous Media

Boming Yu

Dept. of Physics and The State Key Laboratory of Plastic Forming and Die & Mold Technology,
Huazhong University of Science and Technology, Wuhan, 430074, P. R. China

Wei Liu

Dept. of Power Engineering, Huazhong University of Science and Technology, Wuhan, 430074, P. R. China

*A fractal analysis of permeabilities for porous media, both saturated and unsaturated, is presented based on the fractal nature of pores in the media. Both the fractal-phase permeability and the fractal relative permeability are derived and found to be a function of the tortuosity fractal dimension, pore-area fractal dimension, phase fractal dimension, saturation, and microstructural parameters. The proposed models for permeabilities—both the phase permeability and the relative permeability—do not contain any empirical constant. The validity of the present analysis is verified by a comparison with the existing measurements, and excellent agreement between the model predictions and experimental data is found. In addition, the present work reveals that the relative permeability depends not only on saturation but also on the two fractal dimensions, pore fractal dimension (at porosity greater than 0.90), and tortuosity fractal dimension, which characterize the fractal characters of capillaries in porous media. The two fractal dimensions may be the two of the important mechanisms affecting the relative permeability in porous media, and this is a supplement to the available conclusion on relative permeability. © 2004 American Institute of Chemical Engineers *AIChE J*, 50: 46–57, 2004*

Keywords: fractal, permeability, porous media, multiphase flow

Introduction

The permeabilities for porous media, both saturated and unsaturated, have received much attention (De Wiest, 1969; Bear, 1972; Bowles, 1984; Jumikis, 1984; Kaviani, 1995; Panfilov, 2000) due to practical applications, including chemical engineering, soil science and engineering, oil production, polymer composite molding, and heat pipes. Since the microstructures of porous media are usually disordered and extremely complicated, this makes it very difficult to analytically find the permeability of the media, especially for unsaturated (or multiphase) porous media.

Conventionally, the permeabilities of porous media were found by experiments (Levec et al., 1986; Sasaki et al., 1987; Wang et al., 1994; Wu et al., 1994; Shih and Lee, 1998; Chen et al., 2000). Besides, much effort was also devoted to numerical simulations of permeabilities for porous media. Simacek and Advani (1996) performed the numerical solution by reducing a two-dimensional problem to a one-dimensional equation. Adler and Thovert (1998) applied a fourth-order finite difference scheme for permeabilities of real Fontainebleau sandstone. Although no adjustable parameter was involved, a large discrepancy between the average numerical permeability (plotted against porosity) and the experimental data was observed. Ngo and Tamma (2001) applied the finite-element method to calculate the permeability for the porous fiber mat by assuming the Stokes flow in the intertow region and the Brinkman's flow inside the tow region. Compared with single-phase (or satu-

Correspondence concerning this article should be addressed to B. Yu at yu3838@public.wh.hb.cn.

rated) flow in porous media, the multiphase (or unsaturated) immiscible flows in porous media are not well understood. The multiphase immiscible flows in porous media are very important in practical applications such as the petroleum industry, chemical engineering, and soil engineering. The lattice Boltzmann method (LBM) (Benzi et al., 1992; Sahimi and Mukhopadhyay, 1996; Martys and Chen, 1996; Chen and Doolen, 1998), based on the Navier-Stokes equation coupled with Darcy's law, has been extensively used to simulate multiphase flows through porous media in order to understand the fundamental physics associated with enhanced oil recovery, including relative permeabilities. The LBM is particularly useful for complex geometrical boundary conditions and varying physical parameters. However, the results either from numerical simulations or from experiments are usually expressed as correlations with one or more empirical constants, or as curves, and the mechanisms behind the phenomena are thus often ignored. In order to get a better understanding of the mechanisms for permeability, the analytical solution for permeability of porous media becomes a challenging task.

Recently, Yu and Lee (2000) developed a simplified analytical model for evaluating the permeabilities of porous fabrics used in liquid composite molding. This permeability model, which is related to porosity and architectural structures of porous fabrics, is based on the one-dimensional (1-D) Stokes flow in macropores between fiber tows and on the 1-D Brinkman flow in micropores inside fiber tows. Good agreement between theoretical predictions and experimental results was found. However, this model may only apply to those media whose macropores can be simplified as one-dimensional channels. So this and several other models may not be applicable to random/disordered porous media. In addition, this model is only suitable for saturated porous media.

Ransohoff and Radke (1988) applied the circular and triangle capillary models to numerically simulate the flow resistance for laminar flow through unsaturated porous media and studied the dependence of flow resistance on corner geometry, surface shear viscosity, and contact angle.

Katz and Thompson (1985) presented experimental evidence indicating that the pore spaces of a set of porous sandstone samples (in nature) are fractals and are self-similar over 3 to 4 orders of magnitude in length extending from 10 Å to 100 μm. They argued that the pore volume is a fractal with the same fractal dimension as the pore-rock interface. This conclusion was supported by correctly predicting the porosity from the fractal dimension, which was measured by a log-log plot of a number of pores vs. the pore size, and a fractal correlation, $\phi = C(l_1/l_2)^{3-D_f}$, is presented to correlate the measurements on a variety of porous sandstone samples (pores). In the correlation, ϕ is the porosity of porous sandstone, D_f ($= 2 \sim 3$ in three dimensions) is the fractal dimension of pores, C is a constant of order one, and l_1 and l_2 are the lower and upper limits, respectively, of the self-similar regions. Krohn and Thompson (1986) also carried out the experiments on sandstone, and the fractal dimensions of the five sandstone pores were found to be in the range of 2.55–2.85 in three dimensions. Figure 1 (Krohn and Thompson, 1986) displays one of the fractal scaling laws of five sandstone pores. In the figure, the negative slope of the solid line gives the fractal dimension $D = 2.75$ obtained by fitting the measurements from the automatic technique. This figure shows that the sandstone pores are fractal objects in

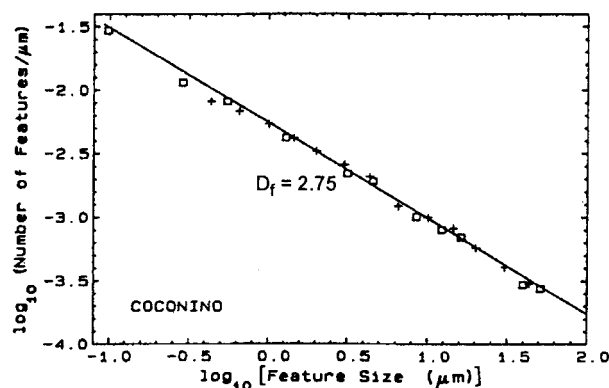


Figure 1. Fractal scaling law from measurement of Cocconino sandstone pores by the automatic technique (Krohn and Thompson, 1986).

nature. Readers may also consult the paper by Krohn and Thompson (1986) for more evidence that the porous media are fractals in nature.

Smidt and Monro (1998) performed experimental investigations on the images of laboratory-made synthetic sandstone and on modeled sandstone. Their results showed that the pore space of both the synthetic and the modeled sandstone was found to be fractals and the fractal scaling laws were obtained by the box-counting method (see Figure 2). Figure 2 presents the fractal scaling law for the laboratory synthetic stone pores, and the slope of the $\log(N_d) \sim \log(1/d)$ plot shows fractal dimension 1.89 (in two dimensions) obtained by the box-counting method (count the number, N_d , of boxes of side length d for covering the pore space). This suggests that the laboratory synthetic stone pores are also fractal objects.

According to the fractal character of real porous media, Yu and Cheng (2002) developed a fractal permeability model for bidispersed saturated porous media (see Figure 3), and this fractal model is also applicable to porous fabrics (Yu et al., 2002) (see Figure 4; Yu et al., 2001). It is seen that the random porous fabric is also a fractal medium. For more fractal microstructures of fabrics, readers may consult the paper by Yu et al. (2001). Although this model does not contain any empirical constant, and good agreement is found between the model predictions and experimental data, it does not apply to unsaturated porous media. The saturated porous medium is, in fact, only the special case of the unsaturated porous medium. It is therefore more meaningful for practical applications to develop an analytical solution for the permeability of unsaturated (or multiphase) porous media. Once the credible permeability is obtained, it also can be used to analyze the heat and mass transfer in unsaturated porous media such as soil (Liu et al., 1995, 1998).

In this article, we focus our attention on the derivation of an analytical fractal model for both the phase and relative permeability of two-phase porous media based on the available evidence that porous media in nature are fractal objects (Katz and Thompson, 1985; Krohn and Thompson, 1986; Young and Crawford, 1991; Perfect and Kay, 1991; Smidt and Monro, 1998; Yu and Li, 2001; Yu et al., 2001, 2002; Yu and Cheng, 2002). This article is organized as follows: the following section describes the fractal characteristics of microstructures of

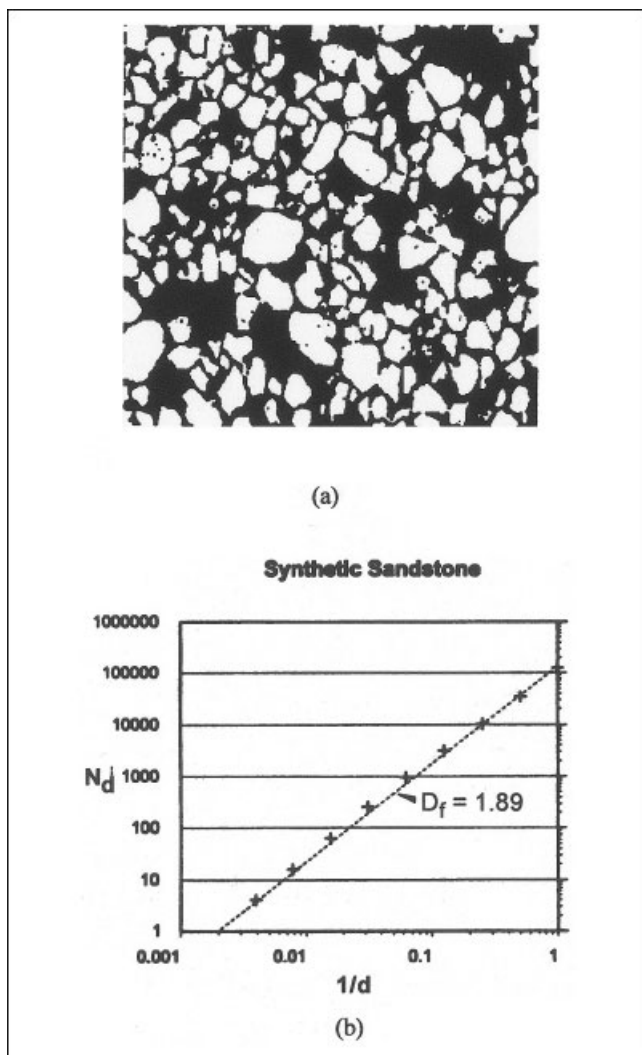


Figure 2. (a) Image of the laboratory-made synthetic sandstone (the white are stones and the black are pores), and (b) the fractal scaling law obtained by the box-counting method applied to the image (Smidt and Monro, 1998).

porous media, which are the theoretical bases for the present fractal analysis of permeability for porous media. The complete fractal permeability models for both saturated and unsaturated porous media are given in the third section. The results and discussions are arranged in the fourth section, and then come the concluding remarks.

The Fractal Description of Microstructures of Porous Media

Porous media such as soil, sandstones in an oil reservoir, packed beds in chemical engineering, fabrics used in liquid composite molding, and wicks in heat pipes consist of numerous irregular pores of different sizes spanning several orders of magnitude in length scales. The pore in porous media plays a remarkable role in fluid flow and heat transfer in porous media. The conventional method for description of characteristics of porous media is based on the volume average (Kaviany, 1995)

over the considered medium, and the significant influence of microstructures on flow is thus ignored. Fortunately, the fractal nature of pores and pore fluids may provide us with a better understanding of the mechanisms of flow and transport properties, such as the permeability in porous media.

It is known that the cumulative size-distribution of islands on the earth's surface follows the power law $N(A > a) \sim a^{-D/2}$ (Mandelbrot, 1982), where N is the total number of islands of area (A) greater than a , and D is the fractal dimension of the surface. Mandelbrot (1982) also pointed out that the sponge gap's (i.e., pores) size distribution is analogous to islands and clusters and satisfies the cumulative distribution function, $N(L > \lambda) \sim \lambda^{-D}$. Majumdar and Bhushan (1990) used this

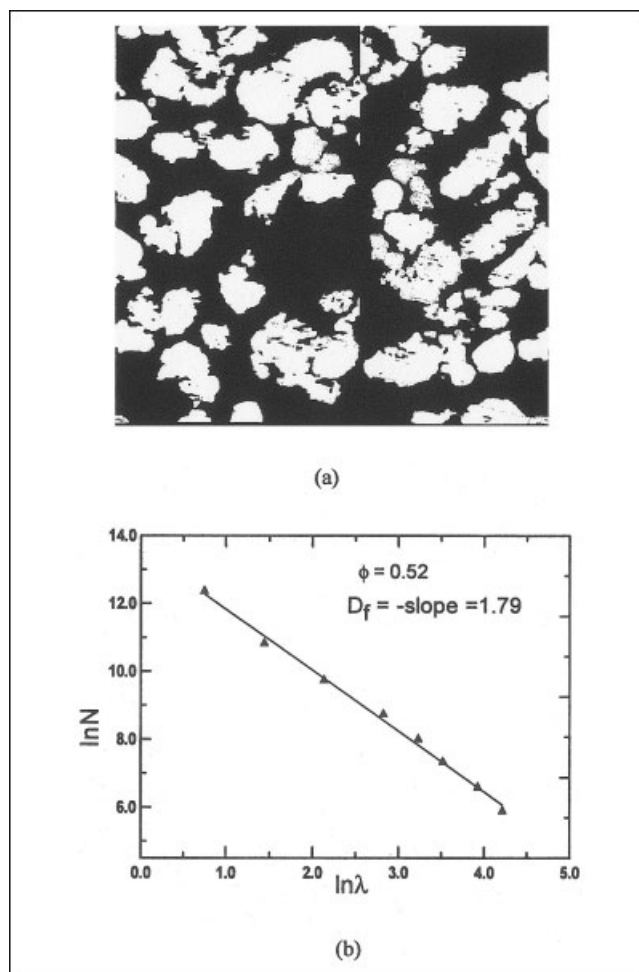


Figure 3. (a) Image photo (Yu and Cheng, 2002) of a bidispersed medium at porosity 0.52, where the black and the white regions are pores and clusters formed by agglomeration of copper particles; since the micropores inside clusters are very small and the copper particles are soft, it is difficult to see the micropores inside clusters after the sample has been polished, and (b) the fractal scaling law obtained by the box-counting method applied to (a) for box number $N(L \geq \lambda)$ vs. box size λ covering the space.

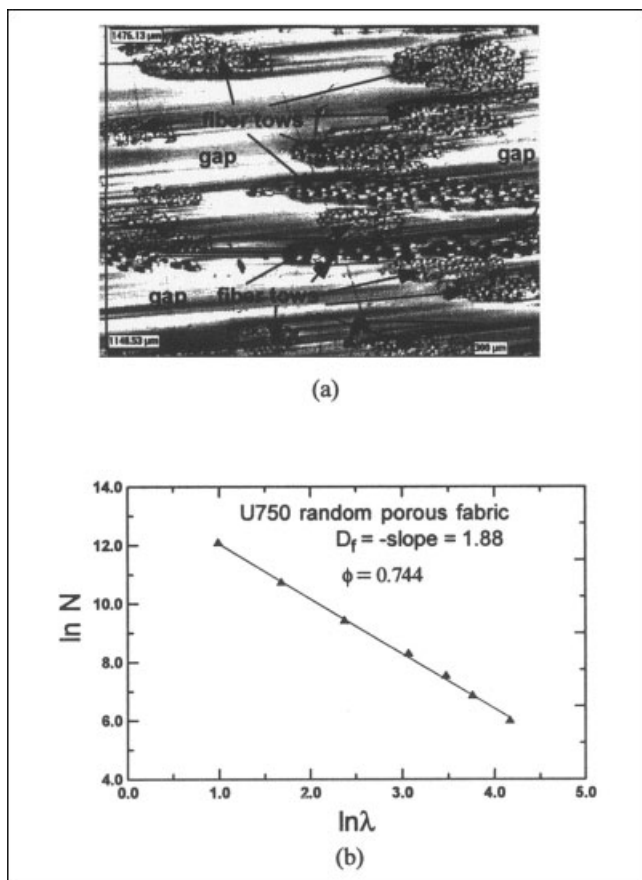


Figure 4. (a) Image photo of the U750 random porous fabric after magnification of 100, and (b) the fractal scaling law obtained by the box-counting method applied to (a) for box (pore) number $N(L \geq \lambda)$ vs. box (pore) size λ covering the space (Yu et al., 2001).

power law to describe the contact spots on engineering surfaces, and the power-law relation is

$$N(A \geq a) = \left(\frac{a_{\max}}{a}\right)^{D_f/2} \quad (1)$$

where $a_{\max} = g\lambda_{\max}^2$, $a = g\lambda^2$, with λ being the diameter of a spot and g being a geometry factor. Compared with the islands on earth or spots on engineering surfaces, the pores in porous media are also analogous to the islands on earth and to the spots on engineering surfaces. The cumulative size-distributions of pores whose sizes are greater than or equal to λ have been proven to follow the fractal scaling law

$$N(L \geq \lambda) = \left(\frac{\lambda_{\max}}{\lambda}\right)^{D_f} \quad (2)$$

where D_f is the pore-area fractal dimension, $1 < D_f < 2$, and λ_{\max} is the maximum pore size. The fractal power-law behavior (Eq. 2) has been proven to be correct by correlating the data from the box-counting method applied to a number of real

porous medium samples with significantly different microstructures (Yu et al., 2001; Yu and Li, 2001; Yu and Cheng, 2002; Yu et al., 2002). For more about the nature of fractals of porous media, readers may also consult the references by Katz and Thompson (1985), Krohn and Thompson (1986), Young and Crawford (1991), Perfect and Kay (1991), Smidt and Monro (1998).

Differentiating Eq. 2 with respect to λ results in the number of pores whose sizes are within the infinitesimal range λ to $\lambda + d\lambda$

$$-dN = D_f \lambda_{\max}^{D_f} \lambda^{-(D_f+1)} d\lambda \quad (3)$$

where $d\lambda > 0$. The negative sign in Eq. 3 implies that the island or pore number decreases with the increase in island or pore size, and $-dN > 0$. The number of pores from Eq. 2 becomes infinite as $\lambda \rightarrow 0$, which is one of the properties of fractal objects (Mandelbrot, 1982). Equation 2 describes the scaling relationship of the cumulative pore population. The total number of pores or islands or spots, from the smallest diameter λ_{\min} to the largest diameter λ_{\max} , can be obtained from Eq. 2 as (Yu and Li, 2001; Yu and Cheng, 2002)

$$N_t(L \geq \lambda_{\min}) = \left(\frac{\lambda_{\max}}{\lambda_{\min}}\right)^{D_f} \quad (4)$$

Dividing Eq. 3 by Eq. 4 gives

$$-\frac{dN}{N_t} = D_f \lambda_{\min}^{D_f} \lambda^{-(D_f+1)} d\lambda = f(\lambda) d\lambda \quad (5)$$

where $f(\lambda) = D_f \lambda_{\min}^{D_f} \lambda^{-(D_f+1)}$ is the probability density function, which satisfies the following condition

$$f(\lambda) \geq 0 \quad (6)$$

Patterned after probability theory, the probability density function, $f(\lambda)$, should satisfy the following relationship

$$\int_0^{\infty} f(\lambda) d\lambda = \int_{\lambda_{\min}}^{\lambda_{\max}} f(\lambda) d\lambda = 1 - \left(\frac{\lambda_{\min}}{\lambda_{\max}}\right)^{D_f} \cong 1 \quad (7)$$

It is clear that Eq. 7 holds if and only if (Yu and Li, 2001)

$$\left(\frac{\lambda_{\min}}{\lambda_{\max}}\right)^{D_f} \cong 0 \quad (8)$$

is satisfied. Equation 8 implies that $\lambda_{\min} \ll \lambda_{\max}$ must be satisfied for fractal analysis of a porous medium; otherwise, the porous medium is a nonfractal medium. For example, if $\lambda_{\min} = \lambda_{\max}$, both Eqs. 7 and 8 do not hold. Equation 8 can be considered to be a criterion of whether a porous medium can be characterized by fractal theory and technique (Yu and Li, 2001). This means that if Eq. 8 does not hold, the porous medium is a nonfractal medium, and the fractal theory and technique are not applicable to the medium. However, in general, $\lambda_{\min}/\lambda_{\max} \sim 10^{-2}$ or $< 10^{-2}$ in porous media, and Eq. 8

holds approximately. Thus, the fractal theory and technique can be used to analyze the characteristics of porous media.

For saturated porous media, the pore area fractal dimension D_f is given by (Yu and Li, 2001)

$$D_f = d - \frac{\ln \phi}{\ln \frac{\lambda_{\min}}{\lambda_{\max}}}, \quad (9)$$

where ϕ is the effective porosity of porous media, $d = 2$ in two dimensions and $d = 3$ in three dimensions. Equation 9 exactly holds for exactly self-similar fractal geometries, such as Sierpinski carpet and Sierpinski gasket (λ_{\max} and λ_{\min} are the upper and lower limits of self-similarity, respectively). However, Eq. 9 approximately holds for random or disordered porous media. For porous media, λ_{\max} and λ_{\min} are the maximum and minimum pore diameters, respectively, in a unit cell or in a sample, implying that the statistical self-similarity exists in the range of $\lambda_{\max} - \lambda_{\min}$ in a porous medium. Equation 9 shows that the pore area fractal dimension is a function of porosity and microstructures, λ_{\min} and λ_{\max} .

A porous medium with various pore sizes can be considered as a bundle of tortuous capillary tubes with variable cross-sectional areas. Let the diameter of a capillary in the medium be λ and its tortuous length along the flow direction be $L_t(\lambda)$. Due to the tortuous nature of the capillary, $L_t(\lambda) \geq L_0$, with L_0 being the representative length. For a straight capillary, $L_t(\lambda) = L_0$. Wheatcraft and Tyler (1988) developed a fractal scaling/tortuosity relationship for flow through heterogeneous media, and the scaling relationship is given by $L_t(\epsilon) = \epsilon^{1-D_T} L_0^{D_T}$ where ϵ is the length scale of measurement. We argue that the diameters of capillaries are analogous to the length scales, ϵ , which means that the smaller the diameter of a capillary, the longer the capillary. Therefore, the relationship between the diameter and length of capillaries also exhibits a similar fractal scaling law

$$L_t(\lambda) = \lambda^{1-D_T} L_0^{D_T} \quad (10)$$

where D_T is the tortuosity fractal dimension, with $1 < D_T < 2$ in two dimensions, representing the extent of the convolutedness of capillary pathways for fluid flow through a medium. Note that $D_T = 1$ represents a straight capillary path, and a higher value of D_T corresponds to a highly tortuous capillary. In the limiting case of $D_T = 2$, we have a highly tortuous line that fills a plane (Wheatcraft and Tyler, 1988). Equation 10 diverges as $\lambda \rightarrow 0$, which is one of the properties of fractal streamlines (Wheatcraft and Tyler, 1988).

Equations 2–3 and 8–10, which provide a complete description of the fractal characteristics of porous media, form the basis of the present fractal analysis of permeabilities, and this will be derived in the following sections.

Fractal Permeabilities for Porous Media

Fractal permeability for saturated porous media

Consider a unit cell consisting of a bundle of tortuous capillary tubes with variable cross-sectional area. The total volumetric flow rate Q through the unit cell is a sum of the flow

rates through all the individual capillaries. The flow rate through a single tortuous capillary is given by modifying the well-known Hagen-Poiseuille equation (Denn, 1980) to give

$$q(\lambda) = G \frac{\Delta P}{L_t(\lambda)} \frac{\lambda^4}{\mu} \quad (11)$$

where $G = \pi/128$ is the geometry factor for flow through a circular capillary, λ is the hydraulic diameter of a single capillary tube, μ is the viscosity of the fluid, ΔP is the pressure gradient, and L_t is the length of the tortuous capillary tube. The total flow rate Q can be obtained by integrating the individual flow rate, $q(\lambda)$, over the entire range of pore sizes from the minimum pore λ_{\min} to the maximum pore λ_{\max} in a unit cell. According to Eqs. 3, 10, and 11, we have

$$Q = - \int_{\lambda_{\min}}^{\lambda_{\max}} q(\lambda) dN(\lambda) = G \frac{\Delta P}{\mu} \frac{A}{L_0} \frac{L_0^{1-D_T}}{A} \frac{D_f}{3 + D_T - D_f} \lambda_{\max}^{3+D_T} \times \left[1 - \left(\frac{\lambda_{\min}}{\lambda_{\max}} \right)^{D_T} \left(\frac{\lambda_{\min}}{\lambda_{\max}} \right)^{3+D_T-2D_f} \right] \quad (12)$$

where D_f is the pore-area fractal dimension, and $1 < D_f < 2$ in two dimensions. Since $1 < D_T < 2$ and $1 < D_f < 2$, the exponent $3 + D_T - 2D_f > 0$ and $0 < (\lambda_{\min}/\lambda_{\max})^{3+D_T-2D_f} < 1$. Also, according to the Yu and Li's criterion (Yu and Li, 2001), $(\lambda_{\min}/\lambda_{\max})^{D_f} \cong 0$ (because $(\lambda_{\min}/\lambda_{\max}) \sim 10^{-2}$). It follows that Eq. 12 can be reduced to

$$Q = - \int_{\lambda_{\min}}^{\lambda_{\max}} q(\lambda) dN(\lambda) = G \frac{\Delta P}{\mu} \frac{A}{L_0} \frac{L_0^{1-D_T}}{A} \frac{D_f}{3 + D_T - D_f} \lambda_{\max}^{3+D_T} \quad (13)$$

Using Darcy's law, we obtain the expression for the permeability of a porous medium as follows

$$K = \frac{\mu L_0 Q}{\Delta P A} = G \frac{L_0^{1-D_T}}{A} \frac{D_f}{3 + D_T - D_f} \lambda_{\max}^{3+D_T} \quad (14)$$

which indicates that the permeability is a function of the pore-area fractal dimension D_f , tortuosity fractal dimension D_T and structural parameters, A , L_0 and λ_{\max} . Equations 13 and 14 indicate that the total flow rate and total permeability are very sensitive to the macropore λ_{\max} , and the total flow rate and total permeability are mainly determined by the maximum/macropore λ_{\max} . This is consistent with the practical situation.

For straight capillaries, $D_T = 1$, Eqs. 13 and 14 can be reduced to

$$Q = G \frac{\Delta P}{\mu} \frac{A}{L_0} \frac{1}{A} \frac{D_f}{3 - D_f} \lambda_{\max}^4 \quad (15)$$

$$K = G \frac{1}{A} \frac{D_f}{4 - D_f} \lambda_{\max}^4 \quad (16)$$

respectively. Equations 13–16 present the single-phase flow rates and single-phase permeabilities (also called absolute permeabilities). Equations 13–16 indicate that the flow rate and permeability are very sensitive to the maximum pore size λ_{\max} . It is also shown that the higher the fractal dimension D_f , the larger the flow rate and the permeability value. From Eqs. 13–16, it can be seen that the flow rate and the permeability will reach the maximum possible values as the pore-area fractal dimension approaches its maximum possible value of 2. This is consistent with fractal theory. Equations 13–16 are valid not only for isotropic porous media but also for anisotropic porous media. For anisotropic porous media, we only need to calculate the principal permeabilities (Yu et al., 2002) in the principal directions by separately using Eqs. 14 or 16, then finding the other permeability components.

Fractal permeability for unsaturated porous media

We now extend the preceding analysis to the permeability for unsaturated porous media. The unique difference between the saturated and unsaturated porous media is that for saturated porous media there is only a single fluid such as water filled with pores or capillary pathways. In an unsaturated porous media there are at least two different fluids, such as water and gas. Figures 5a and 5b display those typical pores, and Figure 5c shows a simplified model for the cross section of a capillary tube partially filled with water and gas. From Figure 5c, we can obtain the pore volume, V_p , and the volume, V_w , occupied by water or wetting phase as

$$V_p = \pi\lambda^2/4 \quad (17)$$

and

$$V_w = V_p - V_g = \pi\lambda^2/4 - \pi\lambda_g^2/4 \quad (18)$$

respectively, where λ and λ_g are the diameter of a capillary pathway and the diameter of the nonwetting (such as gas) phase pathway, and V_g is the volume occupied by a nonwetting fluid (such as gas). According to the definition for saturation, S_w , we have

$$S_w = \frac{V_w}{V_p} = 1 - \left(\frac{\lambda_g}{\lambda}\right)^2 \quad (19)$$

and

$$S_g = \frac{V_g}{V_p} = \left(\frac{\lambda_g}{\lambda}\right)^2 \quad (20)$$

Obviously, Eqs. 19 and 20 satisfy $S_w + S_g = 1$, which is expected. From Eqs. 19 and 20 the diameter for nonwetting fluid (such as gas) can be expressed as

$$\lambda_g = \lambda\sqrt{S_g} = \lambda\sqrt{1 - S_w} \quad (21)$$

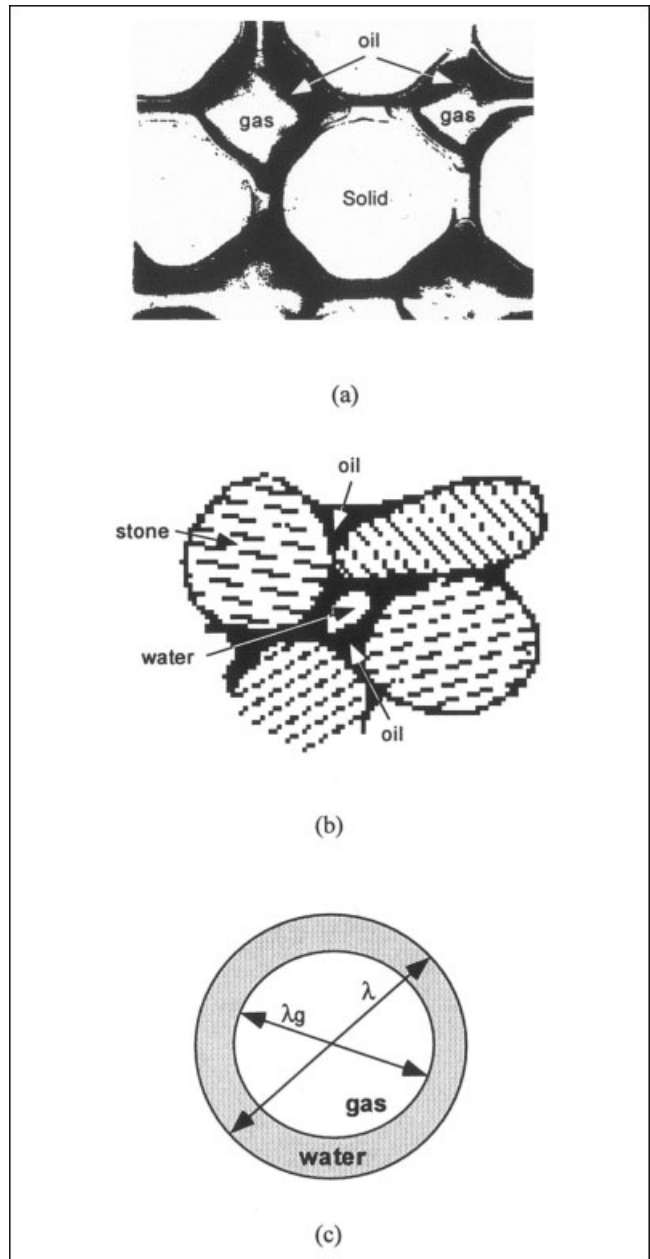


Figure 5. (a) Spontaneous spreading of oil blobs in a capillary (Chatzis et al., 1988), (b) possible fluid saturation state in sandstone (Bear, 1972), and (c) a simplified model for the cross section of a capillary tube partially filled with water and gas.

Equation 21 denotes that $\lambda_g = 0$ as $S_w = 1$ and $\lambda_g = \lambda$ as $S_w = 0$, and vice versa. This is expected and is consistent with the physical situation.

The volume, V_w , occupied by the wetting fluid (such as water) can be written as

$$V_w = \pi\lambda^2/4 - \pi\lambda_g^2/4 = \pi\lambda_w^2/4 \quad (22)$$

where λ_w is the effective diameter of wetting fluid occupying the cross section of a capillary pathway. Again, according to the definition of saturation

$$S_w = V_w/V_p = \lambda_w^2/\lambda^2 \quad (23)$$

This results in

$$\lambda_w = \lambda \sqrt{S_w} \quad (24)$$

Equation 24 indicates that $\lambda_w = 0$, as $S_w = 0$, and $\lambda_w = \lambda$, as $S_w = 1$, and vice versa. This is again expected and is consistent with the physical situation. Usually, $0 < S_w < 1$, such as saturation in soil, in which pores are partially filled with fluid such as water, that is, the two phases (such as water and gas) coexist in soil. From Eqs. 21 and 24, we can directly write the effective maximum and the smallest diameters for wetting and nonwetting fluids in the largest and smallest pores (or capillary tubes) as

$$\lambda_{\max,w} = \lambda_{\max} \sqrt{S_w} \quad (25)$$

$$\lambda_{\min,w} = \lambda_{\min} \sqrt{S_w} \quad (26)$$

$$\lambda_{\max,g} = \lambda_{\max} \sqrt{1 - S_w} \quad (27)$$

$$\lambda_{\min,g} = \lambda_{\min} \sqrt{1 - S_w} \quad (28)$$

The volume fractions, ϕ_w and ϕ_g , for the wetting phase and the nonwetting phase fluids in a unit cell are given by (Bear, 1972)

$$\phi_w = \phi S_w \quad (29)$$

$$\phi_g = \phi(1 - S_w) \quad (30)$$

respectively, and clearly $\phi_w + \phi_g = \phi$.

The permeations of both wetting and nonwetting fluids play important roles in unsaturated (or multiphase) porous media. Muskat and Meres (1936) recommended that the phase permeabilities K_w and K_g be treated as isotropic and given by

$$K_w = K k_{rw} \quad (31)$$

$$K_g = K k_{rg} \quad (32)$$

or

$$k_{rw} = K_w/K \quad (33)$$

$$k_{rg} = K_g/K \quad (34)$$

where K is the absolute permeability (given by Eq. 14) used in the single-phase flows, and k_{rw} and k_{rg} are the relative permeabilities of the w and g phases, respectively.

In this work, the single-phase fractal permeability Eq. 14 is extended to the phase fractal permeabilities, K_w and K_g (k_{rw}

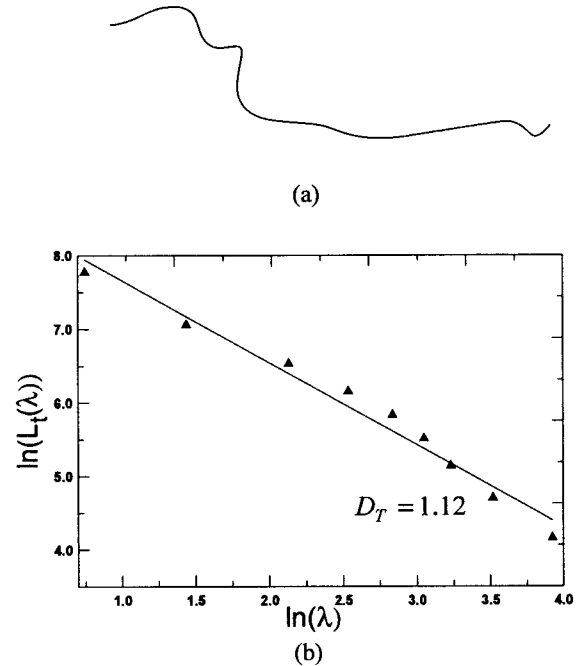


Figure 6. (a) One of possible tortuous streamlines passing through the bidispersed porous medium, and (b) tortuosity fractal dimension, $D_T = 1.12$, measured for (a) by the box-counting method at porosity of 0.52 (Yu and Cheng, 2002).

and k_{rg}), under the following assumptions similar to those by Kaviany (1995):

- (1) The Darcy (Stokes) flow is applicable with a negligible interfacial drag in two-phase porous media.
- (2) The body force is neglected.
- (3) The liquid flow is not coupled with gas flow.
- (4) The viscosities of the liquid and gas phases are independent of each other.

The tortuosity fractal dimension, D_T , is usually determined by the box-counting method or Monte Carlo method, and an analytical expression for D_T has not yet been developed. In this work, we also assume that the wetting and the nonwetting phases flow through tortuous paths have approximately the same tortuosity as the single-phase flow, that is, $D_T = D_{T,w} = D_{T,g} = 1.10$ (Yu and Cheng, 2002) measured using the box-counting method (see Figure 6). Figure 6a depicts one of the possible tortuous streamlines passing through the bidispersed porous medium, and Figure 6b is the fractal scaling law measured by the box-counting method applied to the tortuous streamline. Using the Monte Carlo simulation, Wheatcraft and Tyler (1988) obtained the averaged tortuous streamline fractal dimension $D_T = 1.081$ for flow through heterogeneous media (see Figure 7). Figure 7a demonstrates the simulation results for tortuous streamlines by a fractal random-walk model, and Figure 7b is a plot of fractal travel distance, L_F , vs. the scale of observation, L_s , for the fractal random-walk model. Their Monte Carlo simulation result, $D_T = 1.081$, is very close to the averaged result, $D_T = 1.10$, obtained by the box-counting method (Yu and Cheng, 2002). This work uses $D_T = 1.10$, in calculating permeability.

Applying the analogy between the Darcean single-phase and

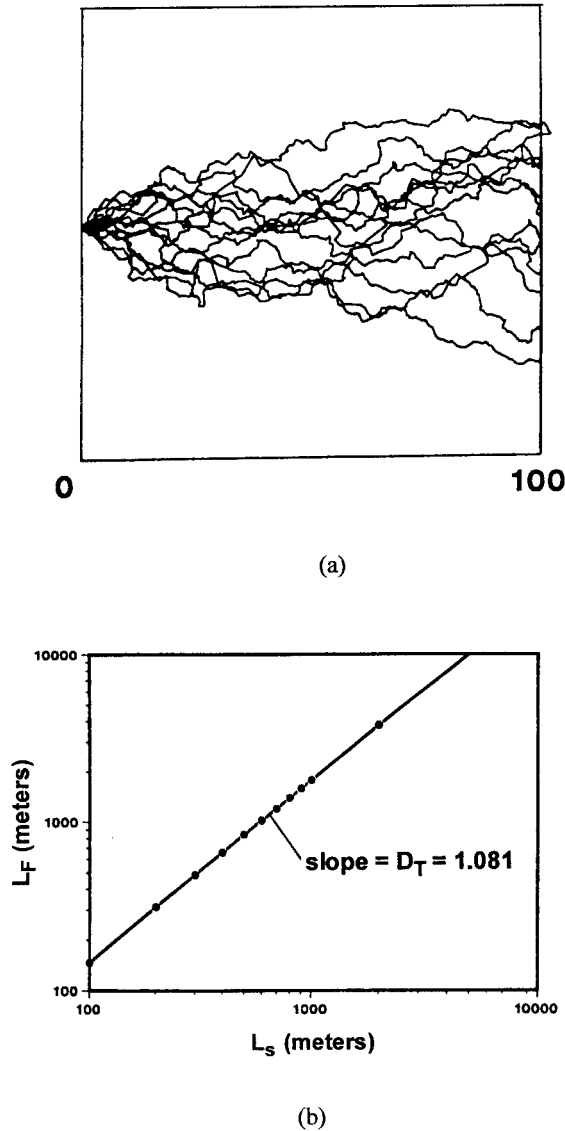


Figure 7. (a) Fractal random-walk model to simulate the flow through heterogeneous medium, and (b) fractal travel distance, L_F , vs. scale of observation L_S for the fractal random-walk model with the averaged tortuosity fractal dimension, $D_T = 1.081$ (Wheatcraft and Tyler, 1988).

two-phase flows, and modifying the single-phase fractal permeability model, Eq. 14, by replacing λ_{\max} in Eq. 14 with Eqs. 25–28, and fractal dimension D_f (Eq. 9) with $D_{f,w}$ and $D_{f,g}$, we can obtain the phase fractal permeabilities for the wetting and nonwetting fluids

$$K_w = G \frac{L_0^{1-D_T}}{A} \frac{D_{f,w}}{3 + D_T - D_{f,w}} \lambda_{\max,w}^{3+D_T}$$

$$= G \frac{L_0^{1-D_T}}{A} \frac{D_{f,w}}{3 + D_T - D_{f,w}} (\lambda_{\max} \sqrt{S_w})^{3+D_T} \quad (35)$$

$$K_g = G \frac{L_0^{1-D_T}}{A} \frac{D_{f,g}}{3 + D_T - D_{f,g}} \lambda_{\max,g}^{3+D_T}$$

$$= G \frac{L_0^{1-D_T}}{A} \frac{D_{f,g}}{3 + D_T - D_{f,g}} (\lambda_{\max} \sqrt{1 - S_w})^{3+D_T} \quad (36)$$

respectively. Equations 35 and 36 reveal that the phase permeability for wetting and nonwetting fluids in porous media is a function of saturation (S_w), fractal dimensions (D_T , $D_{f,w}$, or $D_{f,g}$), and microstructure parameters (λ_{\max} , A , and L_0). It can be seen that the present fractal phase permeabilities do not contain any empirical constant.

In Eqs. 35 and 36, the fractal dimensions $D_{f,w}$ and $D_{f,g}$ can be obtained by extending Eq. 9 and inserting Eqs. 25–30 as

$$D_{f,w} = d - \frac{\ln \phi_w}{\ln \frac{\lambda_{\min,w}}{\lambda_{\max,w}}} = d - \frac{\ln(S_w \phi)}{\ln \frac{\lambda_{\min}}{\lambda_{\max}}} \quad (37)$$

$$D_{f,g} = d - \frac{\ln \phi_g}{\ln \frac{\lambda_{\min,g}}{\lambda_{\max,g}}} = d - \frac{\ln[(1 - S_w) \phi]}{\ln \frac{\lambda_{\min}}{\lambda_{\max}}} \quad (38)$$

Compared with Eq. 37, it is seen that Eq. 9 is only a specific case of $S_w = 1$, and Eq. 37 is a more general form for area fractal dimension in porous media, including the saturated and unsaturated porous media.

We can now turn our attention again on the relative permeabilities for the wetting and nonwetting phases. Noting Eqs. 14, 25–28, 33–36, we arrive at

$$k_{rw} = \frac{K_w}{K} = \frac{3 + D_T - D_f}{3 + D_T - D_{f,w}} \frac{D_{f,w}}{D_f} S_w^{(3+D_T)/2} \quad (39)$$

$$k_{rg} = \frac{K_g}{K} = \frac{3 + D_T - D_f}{3 + D_T - D_{f,g}} \frac{D_{f,g}}{D_f} (1 - S_w)^{(3+D_T)/2} \quad (40)$$

It is evident that the relative permeability is a function of saturation S_w and fractal dimensions D_f , D_T , and $D_{f,w}$ (or $D_{f,g}$), and there is no empirical constant in this fractal relative permeability model.

Results and Discussion

Phase fractal dimensions

The fractal theory requires that the values of fractal dimensions $D_{f,w}$ and $D_{f,g}$ be in the range of 1 and 2 in two dimensions based on the definition given by Eq. 2. To be valid, we first check/calculate the phase fractal dimensions, $D_{f,w}$ and $D_{f,g}$. For this purpose, we take the bidispersed porous media (Yu and Cheng, 2002) as samples for study, because they have been proven to be fractal media. The bidispersed porous structure, as shown in Figure 3a, is composed of clusters (at the macro level), which are agglomerated by small particles (at the micro level). Figure 3b demonstrates the cumulative distribution for pore sizes. The pore-area fractal dimension D_f can be determined by the value of the slope of a linear fit through data on

a log-log plot of the cumulative number of box numbers (pores), $N(L \geq \lambda)$, vs. the box (pore) size, λ .

Since the clusters and particles within the clusters are randomly distributed, this leads to macropores and micropores of various sizes in a bidispersed porous medium. The bidispersed porous media are widely used as wicks in the evaporators of heat pipes. For saturated (or single-phase) bidispersed porous media, the pore-area fractal dimension, D_f , also can be given by Eq. 9 with (Yu et al., 2001; Yu and Cheng, 2002)

$$\frac{\lambda_{\min}}{\lambda_{\max}} = \frac{\sqrt{2}}{d^+} \sqrt{\frac{1-\phi}{1-\phi_i}} \quad (41)$$

where ϕ_i is the porosity inside the clusters, d^+ is the ratio of average cluster size to the minimum particle size, and $d^+ = 24$ (Yu and Cheng, 2002). If we set $\phi_i = 0$, the saturated bidispersed porous media become the saturated monodispersed porous media (such as packed beds), and Eq. 41 is reduced to

$$\frac{\lambda_{\min}}{\lambda_{\max}} = \frac{\sqrt{2}}{d^+} \sqrt{1-\phi} \quad (42)$$

Substituting Eq. 42 into Eq. 9 yields D_f for monodispersed porous media, and inserting Eq. 42 into Eqs. 37 and 38 yields the phase fractal dimensions $D_{f,w}$ and $D_{f,g}$ for unsaturated monodispersed porous media. It should be noted that the monodispersed porous media refer to the materials that consist of particles and pores with different sizes, but these particles do not agglomerate to form clusters. On the other hand, for bidispersed porous media, these particles agglomerate to form clusters with different sizes. The pores in the monodispersed porous media are nonuniform and still follow the fractal scaling law.

The algorithm for determination of the phase fractal dimensions for monodispersed porous media is summarized as follows:

- (1) Select a porosity, ϕ ;
- (2) Find $\lambda_{\min}/\lambda_{\max}$ from Eq. 42;
- (3) Select a saturation, S_w , find $D_{f,w}$ and $D_{f,g}$ (let $d = 2$) from Eqs. 37 and 38.

Procedure 3 is repeated to find the phase fractal dimensions, $D_{f,w}$ and $D_{f,g}$, for a given porosity.

Figure 8 gives the phase fractal dimensions, $D_{f,w}$ and $D_{f,g}$, vs. the saturation, S_w , at different porosities. It is seen from Figure 8 that the phase fractal dimension $D_{f,w}$ increases monotonously with saturation, and as saturation tends to 1, the fractal dimension $D_{f,w}$ reaches its maximum possible value of about 1.80 at porosity 0.54, approximately the same value as that (1.81) for the bidispersed medium (Yu and Cheng, 2002) at porosity 0.54. At present, the explanation for this is that for the monodispersed porous media, Eqs. 37 and 42 are applied to calculate the phase fractal dimension, while for the bidispersed porous media, Eqs. 9 and 41 were used to find the pore area fractal dimension. A similar phenomenon can be observed for the nonwetting fluid. The phase fractal dimension, $D_{f,g}$, reaches its maximum possible value, 1.80, as saturation is zero at porosity 0.54. This means that as saturation tends to zero, the medium is fully filled with a nonwetting fluid (or single-phase fluid), so it is expected that the fractal dimension is exactly the

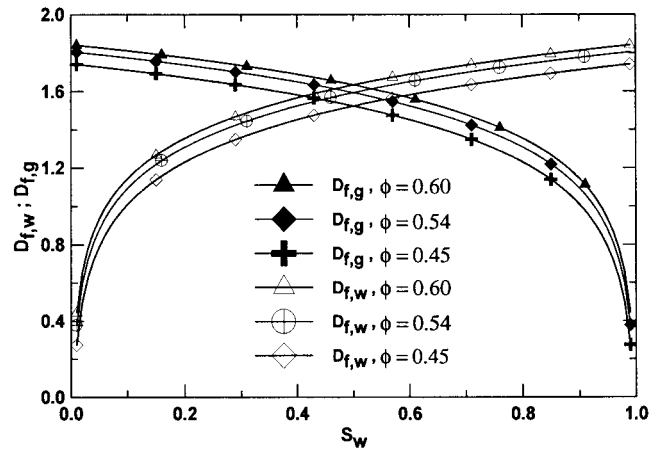


Figure 8. Phase fractal dimensions vs. saturation.

same as that for the saturated porous medium. Figure 8 also shows that the phase fractal dimensions depend on porosity. The higher the porosity, the higher the fractal dimension. One interpretation for this might be that the higher porosity implies larger pore area, and the larger pore area leads to the higher fractal dimension. In the limiting case, as porosity tends to 1, a unit cell of the medium becomes a smooth plane, whose fractal dimension is 2. Therefore, the present results are reasonable. An important phenomenon can be also found from Figure 8. That is when saturation $S_w < 0.1$, the phase fractal dimension $D_{f,w} < 1$. This reveals that when saturation $S_w < 0.1$, the wetting phase distribution in porous media is nonfractal (in two dimensions), according to fractal theory. Similarly, when saturation $S_w > 0.9$, $D_{f,g} < 1$. This means that the nonwetting phase distribution is also nonfractal (in two dimensions) when $S_w > 0.9$. This suggests that only when $S_w > 0.1$ and $S_w < 0.9$, the wetting and nonwetting phases are fractal objects, respectively. On the other hand, according to an article by Kaviani (1995), at very low saturations the wetting phase becomes disconnected (or immobile). At very high saturations, the nonwetting phase becomes disconnected. This means that at low saturation for the wetting phase and at high saturation for the nonwetting phase, the pore fluid is embedded in one dimension and the fractal dimension is less than one, as the fluid is disconnected. Usually, the experimentally relative permeability data (De Wiest, 1969; Bear, 1972; Kaviani, 1995) were also reported in the range of about $S_w > 0.1$ for the wetting phase. Thus, the present fractal analysis of permeability is restricted in the ranges of $S_w > 0.1$ for the wetting phase and $S_w < 0.9$ for the nonwetting phase by the requirements from both fractal theory and experimental observations.

Fractal relative permeabilities

According to the preceding analysis, the present fractal relative permeabilities are given in the ranges of $S_w > 0.1$ for the wetting phase and $S_w < 0.9$ for the nonwetting phase.

The algorithm for determining the relative permeabilities for monodispersed porous media is summarized as follows:

- (1) Select a porosity, ϕ ;
- (2) Find D_f from Eq. 9 with $\lambda_{\min}/\lambda_{\max}$ from Eq. 42;
- (3) Select a saturation, S_w , find $D_{f,w}$ and $D_{f,g}$ from Eqs. 37 and 38;

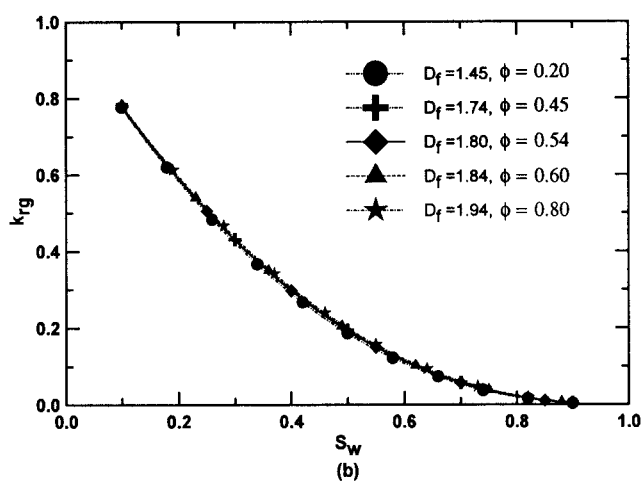
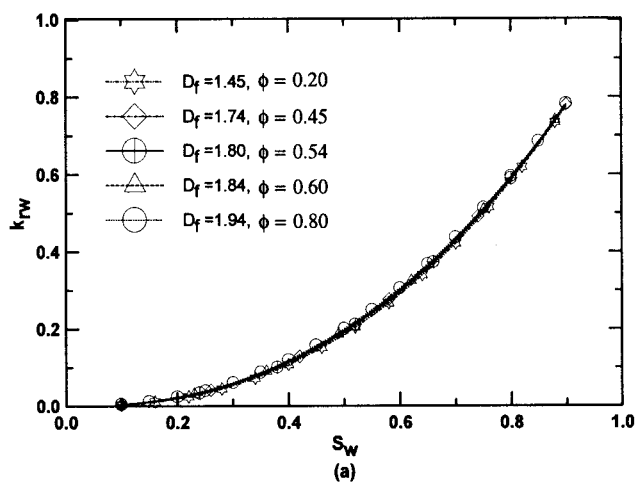


Figure 9. Relative permeabilities predicted by the present fractal model at $D_T = 1.10$: (a) the wetting phase, and (b) the nonwetting phase.

(4) Find the relative permeabilities from Eqs. 39 and 40.

Procedures 3 and 4 are repeated to find the relative permeabilities for a given porosity. In the preceding calculations, we have assumed the tortuous fractal dimension $D_T = D_{T,w} = D_{T,g}$ [= 1.10 from the box-counting method (Yu and Cheng, 2002)]. We have found that this computation of relative permeabilities takes less than one second in a microcomputer, and no grid generation and no boundary conditions are needed. While applying any numerical method such as the finite difference method, finite-element method, lattice-Boltzmann method, and Monte Carlo simulation, grid generation and/or boundary conditions are needed, and thus much more computer time is often required. Therefore, the advantage of the present fractal analysis of permeabilities for porous media over numerical methods is evident.

Figure 9 presents the relative permeabilities, k_{rw} and k_{rg} , vs. saturation at different porosities/pore-area fractal dimensions and at given tortuosity fractal dimension $D_T = 1.10$, calculated from Eqs. 39 and 40, respectively. From Figure 9 it can be found that $k_{rw} + k_{rg} < 1$, which agrees with the general observations, and the shapes of the relative permeability curves are also in agreement with reports in the literature (De Wiest,

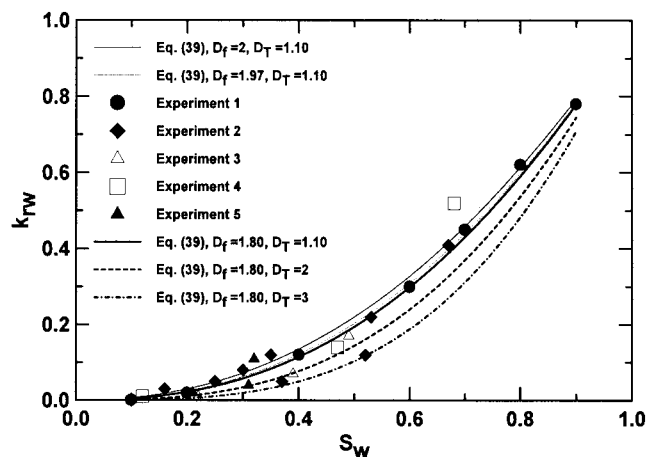


Figure 10. Comparison of the relative permeabilities between the present fractal model predictions and experimental data (see Table 1 for experimental descriptions).

1969; Bear, 1972; Kaviany, 1995). Figure 9 indicates that, although the phase fractal dimensions ($D_{f,w}$ and $D_{f,g}$) depend on porosity (see Figure 8), the relative permeabilities predicted by Eqs. 39 and 40 are independent of the porosity/pore-area fractal dimension, D_f (through Eq. 9), in the porosity range of 0.20–0.80, the usual porosity range, and they depend only on saturation, although the phase permeabilities are dependent upon phase fractal dimensions $D_{f,w}$ and $D_{f,g}$ (see Eqs. 35 and 36). This is consistent with the available conclusions: “the relative permeability depends only on the saturation” and “available experimental evidence indicates that this formal extension and concept of relative permeability that depends only on saturation is a good approximation for all practical purpose” (Bear, 1972). The present fractal relative permeability results are also consistent with the existing correlations (Kaviany, 1995), which are expressed as a function of saturation only, with one or more empirical constants.

Figure 10 compares the predictions from the present fractal permeability model for monodispersed porous media (corresponding to packed beds) to the experimental data (Charpentier and Favier, 1975; Specchia and Baldi, 1977; Saez and Carbonnel, 1985; Levec et al., 1986) for packed beds. See Table 1 for experimental descriptions. It is found that excellent agreement between the predictions from the fractal relative permeability model and the experimental data is obtained at $D_f = 1.80$ (that is, $\phi = 0.54$; note that Eq. 9 relates porosity to pore-area fractal dimension) and $D_T = 1.10$. This verifies the validity of the present fractal analysis of permeabilities for these porous media. However, it should be noted that we choose $D_f = 1.80$ (that is, $\phi = 0.54$) as a reference for comparison because Figure 9 has shown that the relative permeability is independent

Table 1. Experimental Descriptions

Exp.	References	Systems	Packing
1	Levec et al. (1986)	Air–Water	Spheres
2	Charpentier and Favier (1975)	Air–Water	Spheres
3	Favier (1975)	Air–Cyclohexane	Cylinders
4	Specchia and Baldi (1977)	Air–Water	Cylinders
5	Saez and Carbonnell (1985)	Air–Water	Raschig

dent of porosity/fractal dimension D_f in the usual porosity range of 0.20–0.80. Figure 10 further indicates that when fractal dimension D_f is less than 1.97 (i.e., porosity $\phi < 0.90$ calculated by Eq. 9), the relative permeability is independent of porosity/fractal dimension D_f at a given $D_T = 1.10$. This is consistent with the available conclusion, because the available conclusion states that relative permeability depends only on saturation (Bear, 1972). However, at higher porosity, $D_f > 1.97$ (that is, $\phi > 0.90$), it is found that the relative permeability is a weak function of porosity at a given tortuosity $D_T = 1.10$. In the limit of $D_f = 2$ (that is, $\phi = 1$) and $D_T = 1.10$, we have the maximum possible relative permeability, 9% higher than that in the usual porosity range. An explanation for this is that when porosity increases up to 1 (i.e., $D_f = 2$), a unit cell consists of only one capillary tube with no any impermeable substance inside the unit cell (Yu, 2001; Yu et al., 2002; Yu and Cheng, 2002). So, in this situation, the flow resistance reaches the minimum value and the relative permeability arrives at the maximum value. The present result reveals that at higher porosity, $\phi > 0.90$, the relative permeability weakly depends on porosity/fractal dimension D_f , and increases with porosity/fractal dimension D_f . This dependence of relative permeability on porosity/fractal dimension D_f at higher porosity, however, was not reported by experiments and numerical simulations (such as the lattice Boltzmann method), and this article reports such dependence for the first time. Figure 10 also compares the present model predictions to the experimental data in the limit cases of tortuosity fractal dimensions $D_T = 2$ and $D_T = 3$. It is known that the streamlines/capillary tubes/flow fields in porous media exhibit multidimensionality and are similar to turbulence and are often approximately described by turbulence theory (Bear, 1972; Kaviany, 1995). While turbulence can be characterized by fractal theory (Falconer, 1985; Feder, 1988; Turcotte, 1988; Screenivasan, 1991). Thus, the tortuosity fractal dimension, D_T , defined by Eq. 10 may be in the range of 1–2 in a two-dimensional section or in the range of 2–3 in a three-dimensional space. In the limit case of $D_T = 2$, the streamlines/capillary tubes are so tortuous that they fill a plane, while in the limit case of $D_T = 3$, the streamlines/capillary tubes are so tortuous that they fill a three-dimensional space. These limit cases lead to the highest resistance for flow, and thus to the lowest permeabilities. The results show (see Figure 10), that the relative permeabilities are lower (19% and 37%) than the experimental data and the model predictions at $D_f = 1.80$ and $D_T = 1.10$ when the tortuosity fractal dimension D_T increases up to 2 and 3, respectively. This shows that the higher the tortuosity fractal dimension, D_T , the lower the relative permeability. This can be interpreted as the higher tortuosity fractal dimension implies the higher tortuosity of streamlines/capillary tubes, causing the higher flow resistance, and thus resulting in the lower relative permeability. This trend also can be seen from Eq. 39, because relative permeability is proportional to $S_w^{(3+D_T)}/2$, and note that saturation $0 < S_w < 1$. The present work thus also quantitatively explains why 3-dimensional permeability is much lower than 2-dimensional permeability (Adler and Thovert, 1993).

It is seen in Figures 9 and 10 that although the present relative permeability model is expressed as a function of the tortuosity fractal dimension, D_T , pore-area fractal dimension, D_f , phase fractal dimensions, $D_{f,w}$ and $D_{f,g}$, and saturation, S_w , it turns out that the model predictions depend only on saturation

S_w , and on tortuosity fractal dimension D_T in the porosity range of $\phi < 0.90$ (i.e., $D_f < 1.97$). At higher porosity $\phi > 0.90$ (that is, $D_f > 1.97$), the relative permeability increases with porosity/pore area fractal dimension D_f . It is also known that the existing relative permeability correlations contain one or more empirical constants with no physical meaning, and the mechanisms behind these constants were ignored. The present work demonstrates that the tortuosity fractal dimension D_T of streamlines/capillaries and pore-area fractal dimension D_f for characterization of the fractal natures of porous media may be two of the important mechanisms affecting the relative permeability in porous media. Therefore, this work is an addition to the conclusion by Bear (1972) and existing correlations (Kaviany, 1995), which indicate that relative permeability depends *only* on saturation.

The relative permeability, of course, may be affected by many other factors, such as viscosity ratio, surface tension, wettability, density ratio, capillary pressure, hysteresis, and contact angle. This article presents a simple model. A more sophisticated model, which is expected to include one or more other factors, might be studied in the future.

Concluding Remarks

A complete fractal analysis of permeabilities for porous media, both saturated and unsaturated, is presented in this article. The phase fractal permeability models, given by Eqs. 35 and 36, are in terms of the tortuosity fractal dimension D_T , pore-area fractal dimension, D_f , phase fractal dimensions, $D_{f,w}$ and $D_{f,g}$, saturation, S_w , and the structural parameters, A , λ_{\max} , L_0 . The fractal relative permeability models given by Eqs. 39 and 40 are expressed as a function of tortuosity fractal dimension D_T , pore-area fractal dimension D_f , phase fractal dimensions $D_{f,w}$ and $D_{f,g}$, and saturation. There is no empirical constant in the present relative permeability models. The fractal permeability model Eq. 14 can be considered as a special case of the unsaturated porous medium by setting $S_w = 1$ in Eqs. 35 and 37 or by setting $S_w = 0$ in Eqs. 36 and 38. The results (at a given D_T) from the present relative permeability models are found to be independent of porosity/pore-area fractal dimension, D_f , and to depend only on saturation in the porosity range of $\phi < 0.90$ (that is, $D_f < 1.97$), which is consistent with the available conclusion and existing experimental data. At a higher porosity of $\phi > 0.90$ (that is, $D_f > 1.97$), the relative permeability is a weak function of the porosity/pore fractal dimension, D_f , and increases with porosity/pore fractal dimension D_f . The present results also show that the higher the tortuosity fractal dimension, D_T , the lower the permeability. The present work reveals that fractal dimension D_f and tortuosity fractal dimension D_T may be two of the important mechanisms affecting the relative permeability in porous media. Therefore, this work is a supplement to the available conclusion by Bear (1972) and existing correlations (Kaviany, 1995), which indicate that relative permeability depends *only* on saturation. If the tortuosity fractal dimension $D_T = 1.10$ is used for real monodispersed porous media (similar to packed beds), the predictions of the relative permeabilities based on the proposed fractal model in the porosity range of $\phi < 0.90$ (that is, $D_f < 1.97$) are found to be in excellent agreement with experimental data. This verifies the

validity of the present fractal analysis of the permeability for porous media.

However, it should be noted that while the fractal model is able to capture the data shown in Figure 10, it might not be the only model. It should also be noted that not all porous media are fractals. The present model is only applicable to the porous media whose pore-size distributions follow fractal scaling laws. Therefore, one must ascertain experimentally that the porous media used in the experiments (reported in Figure 10) are indeed fractal in nature to conclusively demonstrate that the assumption of fractal geometry is indeed correct. Since many other factors, such as viscosity ratio, surface tension, wettability, density ratio, capillary pressure, hysteresis, and contact angle, may affect the relative permeability, a more complicated model than the present one may need to be developed. This article presents a preliminary work, and further study in this area is in progress.

Acknowledgments

This work was supported by the National Natural Science Foundation of China through Grant Number 59976010 and the National Key Basic Research Development Program of China through Grant Number G2000026303.

Literature Cited

- Adler, P. M., and J.-F. Thovert, "Fractal Porous Media," *Transport Porous Media*, **13**, 41 (1993).
- Adler, P. M., and J.-F. Thovert, "Real Porous Media: Local Geometry and Macroscopic Properties," *Appl. Mech. Rev.*, **51**(9), 537 (1998).
- Bear, J., *Dynamics of Fluids in Porous Media*, Elsevier, New York (1972).
- Benzi, R., S. Succi, and M. Vergassola, "The Lattice Boltzmann Equation: Theory and Applications," *Phys. Rep.*, **222**(3), 145 (1992).
- Bowles, J., *Physical and Geotechnical Properties of Soil*, 2nd ed., McGraw-Hill, New York (1984).
- Charpentier, J. C., and E. Favier, "Some Liquid Holdup Experimental Data in Trickle-Bed Reactors for Foaming and Non-Foaming Hydrocarbons," *AIChE J.*, **21**, 1213 (1975).
- Chatzis, L., A. Kantzas, and F. A. L. Dullien, "On the Investigation of Gravity Assisted Insert Gas Injection, Using Micromodels, Long Berea Cores and Computer Assisted Tomography," SPE63rD Meeting, Houston, TX (1988).
- Chen, S., and G. D. Doolen, "Lattice Boltzmann Method for Fluid Flows," *Annu. Rev. Fluid Mech.*, **30**, 329 (1998).
- Chen, Z. Q., P. Cheng, and T. S. Zhao, "An Experimental Study of Two Phase Flow and Boiling Heat Transfer in Bi-Dispersed Porous Channels," *Int. Commun. Heat Mass Transfer*, **27**, 293 (2000).
- De Wiest, R. J. M., *Flow Through Porous Media*, Academic Press, New York (1969).
- Denn, M. M., *Process Fluid Mechanics*, Prentice Hall, Englewood Cliffs, NJ, p. 35 (1980).
- Falconer, K. J., *The Geometry of Fractal Sets*, Cambridge University Press, Cambridge (1995).
- Feder, J., *Fractals*, Plenum Press, New York (1988).
- Jumikis, A. R., *Soil Mechanics*, Krieger, Malabar, FL (1984).
- Katz, A. J., and A. H. Thompson, "Fractal Sandstone Pores: Implications for Conductivity and Pore Formation," *Phys. Rev. Lett.*, **54**, 1325 (1985).
- Kaviany, M., *Principles of Heat Transfer in Porous Media*, 2nd ed., Springer-Verlag, New York, p. 468 (1995).
- Krohn, C. E., and A. H. Thompson, "Fractal Sandstone Pores: Automated Measurements Using Scanning-Electron-Microscope Images," *Phys. Rev.*, **B33**, 6366 (1986).
- Levec, J., A. E. Saez, and R. G. Carbonell, "The Hydrodynamics of Tricking Flow in Packed Beds, Part II: Experimental Observations," *AIChE J.*, **32**, 369 (1986).
- Liu, W., S. W. Peng, and K. Mizukami, "A General Mathematical Modeling for Heat and Mass Transfer in Unsaturated Porous Media: An Application to Free Evaporative Cooling," *Heat Mass Transfer*, **31**, 49 (1995).
- Liu, W., X. X. Zhao, and K. Mizukami, "2D Numerical Simulation for Simultaneous Heat, Water and Gas Migration in Soil Bed Under Different Environmental Conditions," *Heat Mass Transfer*, **34**, 307 (1998).
- Majumdar, A. A., and B. Bhushan, "Role of Fractal Geometry in Roughness Characterization and Contact Mechanics of Surfaces," *J. Tribology*, **112**, 205 (1990).
- Mandelbrot, B. B., *The Fractal Geometry of Nature*, Freeman, New York, pp. 23 and 117 (1982).
- Martys, N. S., and H. Chen, "Simulation of Multicomponent Fluids in Complex Three-Dimensional Geometries by the Lattice Boltzmann Method," *Phys. Rev.*, **E53**, 743 (1996).
- Muskat, M., and A. W. Meres, "The Flow of Heterogeneous Fluid Through Porous Media," *Physics*, **7**, 346 (1936).
- Ngo, N. D., and K. K. Tamma, "Microscale Permeability Predictions of Porous Fibrous Media," *Int. J. Heat Mass Transfer*, **44**, 3135 (2001).
- Panfilov, M., *Macroscale Models of Flow Through Highly Heterogeneous Porous Media*, Kluwer, London (2000).
- Perfect, E., and B. D. Kay, "Fractal Theory Applied to Soil Aggregation," *Soil Sci. Soc. Amer. J.*, **55**, 1552 (1991).
- Ranshoff, T. C., and C. J. Radke, "Laminar Flow of a Wetting Liquid Along the Corners of a Predominantly Gas-Occupied Noncircular Pore," *J. Colloid Interface Sci.*, **121**, 392 (1988).
- Saez, A. E., and R. G. Carbonell, "Hydrodynamic Parameters for Gas-Liquid Co-current Flow in Packed Beds," *AIChE J.*, **31**, 52 (1985).
- Sahimi, M., and S. Mukhopadhyay, "Scaling Properties of a Percolation Model with Long-Range Correlations," *Phys. Rev.*, **E54**(4), 3870 (1996).
- Sasaki, A., S. Aiba, and H. Fukuda, "A Study on the Thermophysical Properties of a Soil," *J. Heat Transfer*, **109**(1), 232 (1987).
- Screenivasan, K. R., "Fractals and Multifractals in Fluid Turbulence," *Annu. Rev. Fluid Mech.*, **23**, 539 (1991).
- Shih, C.-H., and L. J. Lee, "Effect of Fiber Architecture on Permeability in Liquid Composite Molding," *Polym. Compos.*, **19**(5), 626 (1998).
- Simacek, P., and S. G. Advani, "Permeability Model for a Woven Fabric," *Polym. Compos.*, **17**, 887 (1996).
- Smidt, J. M., and D. M. Monro, "Fractal Modeling Applied to Reservoir Characterization and Flow Simulation," *Fractals*, **6**, 401 (1998).
- Specchia, V., and G. Baldi, "Pressure Drop and Liquid Holdup for Two-Phase Concurrent Flow in Packed Beds," *Chem. Eng. Sci.*, **32**, 515 (1977).
- Turcotte, D. L., "Fractals in Fluid Mechanics," *Annu. Rev. Fluid Mech.*, **20**, 5 (1988).
- Wang, T. J., C. H. Wu, and L. J. Lee, "In-Plane Permeability Measurement and Analysis in Liquid Composite Molding," *Polym. Compos.*, **15**(4), 278 (1994).
- Wheatcraft, S. W., and S. W. Tyler, "An Explanation of Scale-Dependent Dispersivity in Heterogeneous Aquifers Using Concepts of Fractal Geometry," *Water Res. Res.*, **24**, 566 (1988).
- Wu, C.-H., T. J. Wang, and L. J. Lee, "Trans-Plane Fluid Permeability Measurement and Its Application in Liquid Composite Molding," *Polym. Compos.*, **15**(4), 289 (1994).
- Young, I. M., and J. W. Crawford, "The Fractal Structure of Soil Aggregations: Its Measurement and Interpretation," *J. Soil Sci.*, **42**, 187 (1991).
- Yu, B. M., and L. J. Lee, "A Simplified In-Plane Permeability Model for Textile Fabrics," *Polymer Compos.*, **21**(5), 660 (2000).
- Yu, B. M., and J. H. Li, "Some Fractal Characters of Porous Media," *Fractals*, **9**(3), 365 (2001).
- Yu, B. M., L. J. Lee, and H. Q. Cao, "Fractal Characters of Pore Microstructures of Textile Fabrics," *Fractals*, **9**, 155 (2001).
- Yu, B. M., "Comments on 'A Fractal Geometry Model for Evaluating Permeabilities of Porous Preforms Used in Liquid Composite Molding,'" *Int. J. Heat Mass Transfer*, **44**, 2787 (2001).
- Yu, B. M., and P. Cheng, "A Fractal Permeability Model for Bi-Dispersed Porous Media," *Int. J. Heat Mass Transfer*, **45**(14), 2983 (2002).
- Yu, B. M., L. J. Lee, and H. Q. Cao, "A Fractal In-Plane Permeability Model for Fabrics," *Polym. Compos.*, **23**(2), 201 (2002).

Manuscript received Nov. 8, 2002, and revision received May 25, 2003.